中國機械工程學刊第四十四卷第六期第 523~532 頁(民國一百一十二年)
Journal of the Chinese Society of Mechanical Engineers, Vol.44, No.6, pp523~532 (2023)

Enhanced Microwave Absorption in Salisbury Screen Absorbers by Incorporating Hybrid Reduced Graphene Oxide Papers

Hsien-Kuang Liu*, Ruey-Bin Yang** and You-Jyun Wu***

Keywords: hybrid, reduced graphene oxide paper, weight fraction, sonication time

ABSTRACT

An innovative hybrid RGO/GO (reduced graphene oxide/graphene oxide) papers, HGOP incorporated in Salisbury screen absorbers are successfully demonstrated. Compared with reduced graphene oxide papers RGOP, HGOP possesses tunable RGO/GO ratio such that several advantages are achieved including better impedance matching between air and HGOP and creation of more loss mechanisms. For fabricating HGOP, important processing parameters include RGO/GO weight fraction in suspension, sonication time for suspension, and thickness of HGOP. For RGO/GO of 1.5 wt%, sonication time of 10 min, HGOP thickness of 0.5 mm, and air spacer thickness of 3.16 mm, the HGOP15–T10–TH5–AS3 radar absorbing structure (RAS) has attained superior reflection loss (RL) of – 49.1 dB at 10.6 GHz with –10 dB bandwidth of 3.9 GHz. To analyze major loss mechanisms caused by this RAS, scanning electron microscope (SEM) micrographs of various HGOP are carefully examined. Functional groups and interaction of RGO/GO are found to be effective for loss mechanisms. Better microwave absorbing properties can be attributed to multiple loss mechanisms of the HGOP and the destructive interference mechanism.

Paper Received July, 2023. Revised October, 2023. Accepted Novenber, 2023. Author for Correspondence:Hsien-Kuang Liu.

**Professor, Department of Mechanical and Computer Aided Engineering, Feng Chia University, Taichung 40724, Taiwan, R.O.C. hkliu@fcu.edu.tw*

*** Professor, Department of Aerospace and Systems Engineering, Feng Chia University, Taichung 40724, Taiwan, R.O.C. rbyang@fcu.edu.tw*

****Graduate Student, Department of Mechanical and Computer Aided Engineering, Feng Chia University, Taichung 40724, Taiwan, R.O.C.*

INTRODUCTION

The radar absorbing structures (RASs) proved successfully in the early age of the 20th century for military purposes. Nowadays RASs have evolved and applied prevalently for human life including not only warplanes and warships, but also anti-radiation devices, clothes, and building. Due to advancement of material technology, light weight, wide bandwidth, thin thickness and flexibility of excellent RASs (Yang, 2014; Zhang, 2014) become achievable to conceal sensitive great bodies like planes, battle ships, tanks, and military equipment by enhancing electromagnetic reflection losses (Houbi, 2021). Besides, RASs significantly reduced radar cross section (RCS) of an object in specific radar frequency band and were used in the strategic area of camouflage and stealth technology (Zhao, 2014). A larger RCS indicates that an object is more easily detected by radar. Microwave absorbing materials (MAMs) can be classified based on their loss mechanisms, including dielectric-loss dominated MAMs such as SiO_2 ceramics, magnetic-loss dominated MAMs such as magnetic metal oxide, and conductive-loss dominated MAMs such as carbon materials (Pang, 2021). Usually, an effective MAM combine two or three loss mechanisms. Among them, nanomaterials become an excellent candidate for MAMs due to their high specific area and other advantages.

Nanomaterials used as microwave absorbents could exhibit good absorbing performance and low filler content, including graphene nanosheets, carbon nanotubes (CNTs), carbon nanofibers, nanoparticles, and nanospheres due to their size and micro-structures (Zhang, 2018; Pan, 2017; Wen, 2014). Choudhary et al. (2017, 2019, 2021) have adopted a single-step pyrolysis method in synthesizing carbon globules at 800°C or 1000°C, using metal (Fe-, Ni-, Mn-, or Co-) organometallic precursors. Then those carbon globules consisting of graphite coated metallic nanoparticles such as nanoscale iron/iron-carbide graphite (FeC) particles, were combined with PVDF to achieve composite materials with good performance for EMI shielding or microwave absorption. The PVDF–FeC composite showed an excellent reflection loss of −40.5 dB for a 4.3 mm thick specimen positioned at 5 GHz frequency. Synergetic microwave absorption of those composites was caused via dielectric, magnetic and conductive losses.

RGO and RGO composites are major promising materials that are adopted for microwave absorption applications (Xu, 2015; Meng, 2018). Their related technologies are collected and discussed here. (1) fabrication of RGO: Wu et al. (2015) adopted a hydrothermal process to reduce GO (graphene oxide) to RGO (reduced graphene oxide) aerogel. A hydrothermal process is a method of producing RGO in which a solvent containing GO nanosheets is put under high pressure and temperature in an autoclave. Only with a very low filler loading (10 wt%), the S(spongelike)-PPy(polypyrrole)/RGO aerogel based composite could reach an effective electromagnetic absorption (EA) bandwidth (below −10 dB) of 6.76 GHz, and the highest reflection loss reached −54.4 dB at 12.76 GHz. Ren et al. (2021) reported a facile solvothermal method to construct Fe_3O_4/RGO composites. Solvothermal synthesis is a method of producing chemical compounds in which a solvent containing reagents of Fe_3O_4 and RGO is put under high pressure and temperature in an autoclave. The composite showed a minimum reflection loss of −64.7 dB at 6.6 GHz with an absorber thickness of 4.5 mm and a broad effective absorption bandwidth of 13.6 GHz with the thickness of 1.5–5 mm. Li et al. (2020) adopted a similar method to fabricate RGO/NZCF/paraffin wax composites. The reflection loss of composites was excellent, with a value of −47.10 dB and ultralow thickness of only 0.44 mm, and the maximum bandwidth reached 3.7 GHz with merely 1.5 mm in thickness. As microwave absorbers, RGOs were usually used as fillers to polymers (e.g., epoxy resin) to make RGO-reinforced nanocomposites (Chen, 2017) because they can replace magnetic metal powder absorbers and reduce both weight and thickness. In this work, RGO is reduced from GO by putting GO in a high temperature furnace at 1000^{o}C. However, sole nano-scale RGO suffered from poor dispersion in the matrix. (2) fabrication of RGO composites: The RGO nanosheets can be simply mixed with epoxy resin or magnetic materials to achieve the composites (Xu, 2015; Meng, 2018; Chen, 2017). Or RGO and magnetic materials can be combined together by a solvothermal synthesis (Ren, 2021). (3) fabrication of RGO paper: The RGO nanosheets can simply combined together as a RGO paper by the vacuum filtration method (Dikin, 2007; Park, 2012; Liu, 2022). Details of steps are described in section 2.1. The RGO paper itself can be served as a microwave absorber, or it can be made as a RAS.

RGOP can preserve most properties that the monolayer RGO possesses, and are even more suitable for RASs due to its robustness, large area, and low thickness. The RGOP RAS incorporated with glass fabric composite was fabricated by authors and exhibited reflection loss of −37.4 dB at 11.8 GHz with total thickness of only 2.76 mm (Liu, 2022). Recently, metamaterials (Pang, 2021) attracted much attention by their unnatural electric and magnetic properties, which is mainly attributed to their special artificial structures. The periodically structure helps to obtain excellent microwave absorbing properties which are far beyond that of general MAMs, and even some lossless materials can show huge microwave absorption.

For application in widespread fields, robust properties of either GO or RGO papers are important. Wang et al. (2013) adopted the focus ion beam (FIB) method to fabricate GOP micrometer beams, and found that tensile strengths of the beams increase with the decrease of width. This result is correlated with inter nanosheet defects of the paper. Park et al. (2012) fabricated the RGOP from the RGO suspension by filtration method, and found that the lowest concentration of suspension leads to the highest Young's moduli and fracture strengths of more flat RGOPs. On the other hand, the highest concentration of suspension results in higher electrical conductivity of RGOP because of the agglomerated effect of RGO nanosheets. Dikin et al. (Dikin, 2007) adopted GO (graphene oxide) suspension and vacuum filtration method to fabricate GO papers. After five fatigue loading cycles, the elastic modulus of GO papers increases 20%. Effects of processing parameters on fatigue lives of GOP were ever investigated (Liu, 2020). The longest fatigue life was achieved for the GOP under highest power sonication time and lowest graphene weight fraction in GO suspension.

In this paper, we adopt hybrid RGO/GO papers termed HGOP composed of interlocked GO and RGO nanosheets to replace the resistive 377 Ω/sq sheet in the Salisbury screen type absorber for fabricating a novel thin RAS. This RAS includes a HGOP surface layer, a honeycomb or glass fabric composite as a spacer in the middle, and a perfect conducting layer such as an aluminum foil in the bottom. The HGOP is fabricated by the vacuum filtration method using suspension with various composition of RGO and GO nanosheets in deionized water. Three important processing parameters of HGOP are investigated. Compared with the RGOP, composition of RGO/GO of HGOP is adjustable such that impedance matching of HGOP and air can be optimized and favorable for reflection loss. The electromagnetic properties and microwave absorption characteristics of the HGOP absorbers are investigated at X-band (8.2-12.4 GHz). With the addition of HGOP, the RAS is expected to have the advantages of light weight, wide bandwidth, and flexibility. This HGOP RAS could be served as patch-type radar absorbing films which can be integrated in the curved 3D parts of stealth aircrafts such as the leading edges of wings to reduce the RCS of the jetfighters.

EXPERIMENTAL PROCEDURES

Fabrication of HGOP and Radar Absorbing Structures

To fabricate hybrid RGO/GO papers (HGOP), initially graphene oxide (GO) nanosheets were fabricated by the modified Hummers method. First, 12-gram expanded graphite powders supplied by Homytech Co., Ltd., Taiwan were added in 460-ml H_2SO_4 and this suspension was stirred in an ice bath. Later, 60-gram $KMnO_4$ were slowly added to the suspension, and it was heated to 35°C and stirred for 2 h. Then 920-ml deionized water was slowly added in the suspension and the temperature has to be kept under 50°C. The suspension was further diluted by 2800-ml deionized water, and then 50-ml 30% concentration H_2O_2 was added. The suspension stood still for 24 h. After that, the suspension was set in centrifuge by revolution of 6000 rpm for 1 h to separate solute and solvent. The solute was further purified by the addition of the mixture of water and methanol. Centrifuge and purification processes were repeated for several cycles. After drying, GO nanosheets were acquired.

To achieve reduced graphene oxide (RGO) nanosheets, HMTA (hexamethylenetetramine) suspension was used to reduce GO as RGO. 5 grams HMTA were added in 500 grams de-ionized water (DIW) to make a uniform HMTA suspension. Then the suspension was heated up to 100ºC. Thereafter 5 grams GO nanosheets were added into this HMTA suspension. Later, similar centrifuge and purification processes were also repeated for several cycles. After drying, RGO nanosheets were acquired. To prepare RGO/GO suspension, three combinations of different amount of RGO and GO nanosheets were added in deionized water (DIW) and stirred uniformly. The combination is shown in table 1. For example, for RGO/GO 0.5/1.0wt% in suspension amounts of RGO/GO/DIW are respectively 0.5g/1g/98.5g. Later, three kinds of sonication times were applied in suspensions including 10, 15, and 20 min.

Hybrid RGO/GO papers (HGOP) were fabricated by the vacuum filtration method. 5-ml RGO/GO sonicated suspensions with the various weight fractions were poured into upper container of a vacuum filtration apparatus. Lower container has an outlet that connects with a vacuum pump. There is a filtration assembly consisting of porous glass and cellulose filter paper (provided by Advantec Toyo Kaisha, Ltd., Japan) between upper and lower parts of the apparatus. When the vacuum pump was turned on, the solvent of the RGO/GO suspension was sucked out and HGOP nanosheets were combined as HGOP above filtration assembly. After drying process, a free-standing circular HGOP with diameter 35 mm can be achieved. Figure 1(a) shows the fabricated HGOP. In order to study effect of HGOP thickness on radar absorbing properties, laminate HGOP was fabricated by the addition of adhesion between single HGOPs. A 4 wt% polyvinyl alcohol (PVA) solution was used to adhere papers as a laminate. Thickness of laminate HGOP is controlled in the range of 0.3 to 0.8 mm, and named as TH3 to TH8 as shown in table 1. Table 1 also shows the nomenclature for the various fabricated HGOPs and RAS. Graphene weight fractions in suspension are denoted as HGOP15, 20, and 25 for 1.5 (RGO/GO =0.5/1.0%), 2.0, and 2.5 wt%, respectively; sonication time is denoted as T10, T15, and T20 for 10, 15, and 20 min, respectively; thickness for the HGOP is denoted from TH3 (0.3mm) to TH8, respectively. For example, HGOP15-T10-TH5-AS3 represents the HGOP RAS fabricated with the RGO/GO weight fraction of 0.5/1.0 wt% in suspension (HGOP15), applied sonication time of 10 min (T10), HGOP thickness of 0.5 mm (TH5), and air spacer thickness of 3.16 mm. An experimental process for fabrication of HGOP RAS is depicted in figure 1(b).

Table 1. Nomenclature and composition for various fabricated HGOP and RAS.

	HGOP with various RGO/GO weight fraction in suspension (wt%)	Sonication time (min)	Paper thickness (mm)	Air spacer thickness (mm)
HGOP (Hybrid RGO/GO paper)	HGOP15 (RGO/GO =0.5/1.0%)	T10 (10 min)	TH3 (0.3 mm)	AS1 (1.05 mm)
	HGOP20 (RGO/GO =1.0/1.0%)	T15 (15 min)	TH8 (0.8 mm)	AS2 (2.1 mm)
	HGOP25 (RGO/GO =1.5/1.0%)	T20 (20 min)		AS3 (3.16 mm)

(a)

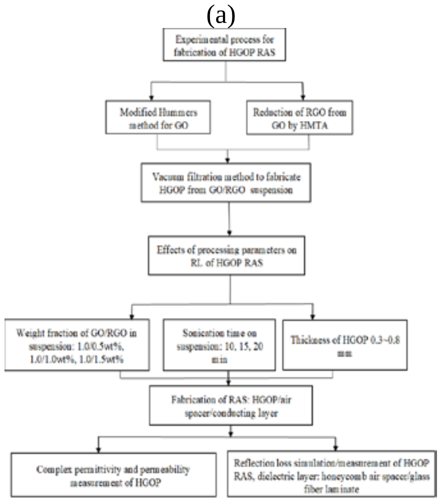

(b)

Fig. 1. (a) The fabricated hybrid RGO/GO paper (HGOP), (b) experimental process for fabrication of HGOP RAS.

Reflection Loss Measurement and Characterization

The reflection loss of the HGOP RAS and the microwave absorbing material characterization of the HGOP layer were performed in a rectangular waveguide by measuring the scattering parameters (S11 and S21) with a vector network analyzer (VNA) as detailed in authors' previous work (Liu, 2022). The HGOP RAS with dimensions of 23.5×11 mm was installed inside the waveguide. The three-layer HGOP RAS consists of HGOP with various thickness from TH3 to TH8, a honeycomb air spacer with various thicknesses of 1.05 mm, 2.1 mm, 3.16 mm, and aluminum foil as perfect conductive layers. A Salisbury screen mechanism of this RAS absorber is explained in figure 2. The absorbing mechanism here includes wave destructive interference, high dielectric and conductive losses of HGOP, and impedance matching to air. The electromagnetic properties (ε', ε", μ', μ") of thin HGOP laminates with dimension 23.5 ×11 mm were measured in the X-band (8.2–12.4 GHz) rectangular waveguide by using Agilent 85071E software which is based on the Nicolson–Ross–Weir (NRW) method. With those properties, Ansys HFSS software was used to simulate the reflection loss and the results were compared with the measured data. In order to understand the correlation between microstructure of HGOP and reflection loss, a scanning electron microscope was employed to carefully observe the cross section of the HGOP.

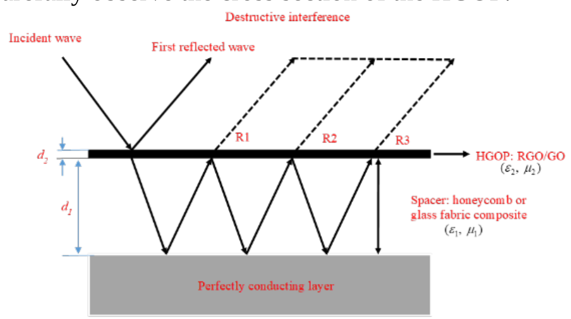

Fig. 2. A HGOP Salisbury screen radar absorbing structure (RAS) and its destructive interference mechanism.

EXPERIMENTAL RESULTS

Effect of RGO/GO Weight Fraction in Suspension

To fabricate HGOP, there are three RGO/GO weight fractions in suspension, i.e. 0.5/1.0, 1.0/1.0, and 1.5/1.0 wt% with fixed amount of GO but gradually increasing amount of RGO. With lowest RGO/GO weight fraction of 0.5/1.0 wt%, figure 3(a) depicts reflection losses for HGOP15–T10–TH5 RAS using three air spacer (honeycomb) thicknesses of 1.05 mm, 2.1 mm, and 3.16 mm. For air spacer thickness of 3.16 mm, the reflection loss peak of the RAS is excellent and found to be – 49.1 dB at a frequency of 10.6 GHz, while RASs with air spacers 1.05 and 2.1 mm have no peak value at X-band frequency. With this RL value, the RAS can absorb 99.99% microwave. Furthermore, this RL value is compared with that in reference (Peng, 2023) using RGO/$MnFe_2O_4$ nanocomposite papers, and found that the former is better than RL of -43.2 dB in the reference.

With higher RGO/GO weight fraction in suspension of 1.0/1.0 wt%, figure 3(b) depicts reflection losses of HGOP20-T10-TH5 RAS in which two kinds of air spacers of 2.1mm and 3.16 mm lead to reflection loss peaks of –18.4 dB at 11.8 GHz and –15.9 dB at 9.7 GHz, respectively. With highest RGO/GO weight fraction of 1.5/1.0 wt% in figure 3(c), HGOP25–T10–TH5 RAS with 3.16 mm air spacer has reflection loss peak value of –23.0 dB at 10.9 GHz.

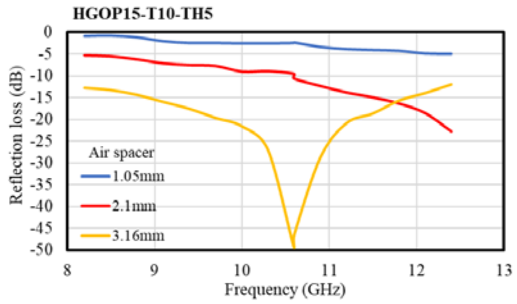

(a)

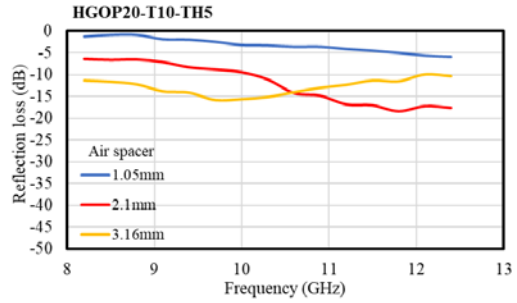

(b)

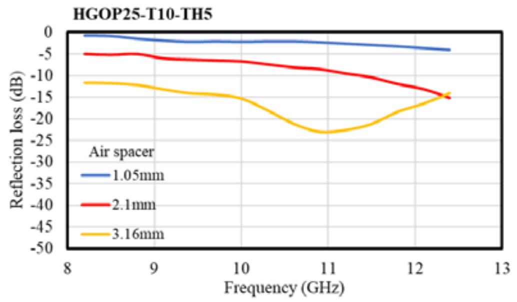

(c)

Fig. 3. Reflection loss for (a) HGOP15-T10-TH5, (b) HGOP20-T10-TH5, (c) HGOP25-T10-TH3 RAS with various spacers.

Figure 4 summarizes the effect of graphene weight fraction in suspension on minimum reflection losses of 9 kinds of HGOP RASs. The reflection losses of around half RASs increase with the increase of graphene weight fraction in suspension. Two factors could result in this trend: one is microstructure evolution and the other is impedance matching of HGOP RAS. For the first factor, figure 5 (a), (b), and

(c) shows micrographs for HGOP15–T10, HGOP20–T10, and HGOP25–T10, respectively, with increasing RGO/GO weight fraction of 0.5/1.0, 1.0/1.0, and 1.5/1.0 %. Two microstructure evolutions are found in HGOPs with gradually increasing weight fraction of RGO in suspension. First, interlayer pore size and number increase, and second edge breakage of HGOP is found for highest RGO weight fraction of 1.5%. The first feature is caused by undulation nature of RGO nanosheets (Liu, 2016). Accumulated effect of stacking more undulated RGO nanosheets for higher RGO weight fraction in the HGOP causes non-uniform microstructure and finally leads to more pores and edge breakage of HGOP. According to our other previous studies (Liu, 2022), lower RGO weight fraction leads to HGOP with dense microstructure, and this is likely to result in HGOP with higher permittivity. Therefore, this complex permittivity leads to higher dielectric loss that can dissipate energy of the incident wave and also allow partial penetration of the wave to the metal-backed reflective layer. With arrangement of proper air spacer thickness of 3.16 mm, good Salisbury screen effect occurs. Therefore, lower RGO weight fraction in suspension increases microwave absorbing ability of HGOP, and leads to minimum reflection loss (RL) – 49.1 dB of HGOP15-T10-TH5-AS3 RAS.

For the second factor of impedance matching, the HGOP RAS shows much better RL of – 49.1 dB than – 26.5 dB of RGOP20–T15–L6 RAS (Liu, 2022). The RGOP RAS adopted RGOP with higher conductivity due to its less oxygen-based functional groups such that incident microwaves partially penetrate and partially reflect from the surface of RGOP. However, this phenomenon is improved by using HGOP composed of RGO/GO because conductivity of GO is low. This lower and tunable conductivity would enhance the impedance matching between HGOP and air and the incident wave would better penetrate the HGOP rather than reflect from the HGOP. More penetration of microwave may lead to multiple reflection inside the RAS as shown in figure 2. This leads to a better Salisbury screen effect in the HGOP RAS compared with RGOP RAS.

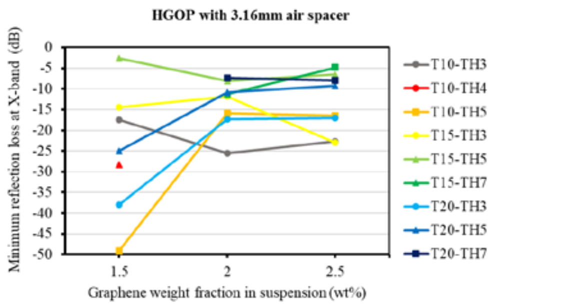

Fig. 4. Effect of graphene weight fraction in suspension on reflection loss of 9 kinds of HGOP RASs.

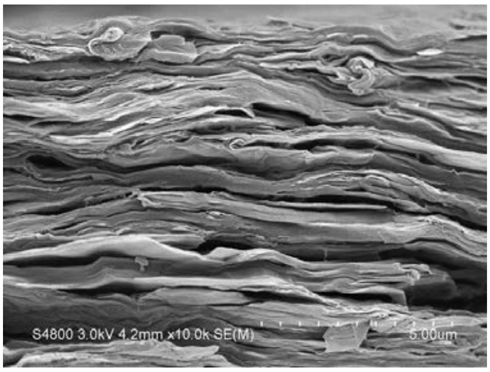

(a)

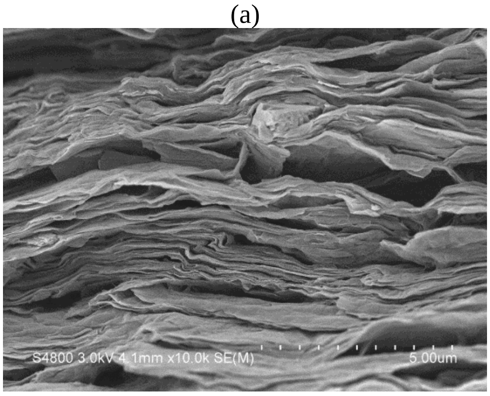

(b)

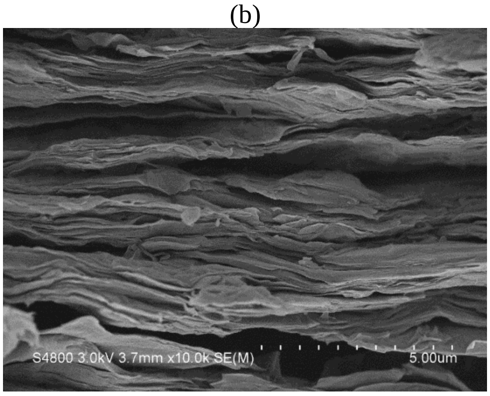

(c)

Fig. 5. Micrographs for (a) HGOP15-T10, (b) HGOP20-T10, (c) HGOP25-T10.

Effect of Sonication Time

Figure 6 shows effect of sonication time of suspension on reflection loss of HGOP15–TH5–AS3 RASs. It seems that peak value of reflection loss approximately increases with the increase of sonication time. With lowest sonication time of 10 min, HGOP15–T10–TH5–AS3 RAS has minimum reflection loss of **–** 49.1 dB; further with the indicated dashed line at **–** 10 dB, it shows good bandwidth of 3.9 GHz. Figure 7 depicts the effect of sonication time of suspension on the minimum reflection losses of 9 kinds of HGOP RASs. As a general trend, the results show that reflection loss of most RASs increase with the increase of sonication in the range of 10 to 20 min, except for HGOP15–TH3. This trend is in contrast to that of RGOP RAS where reflection losses of RGOP RASs decrease with the increasing sonication time. First, due to very low conductivity of GO HGOP has better impedance matching with air compared with RGOP. Second, with longer sonication time on HGOP GO nanosheets inside HGOP are broken as many fragments along both in-plane and out of plane directions. Therefore, this would release a lot of functional groups such as –COOH and –OH attached on GO fragments. As GO has far more functional groups than RGO, those released functional groups would make HGOP similar to insulation. Therefore, microwave would tend to penetrate rather than induce a dielectric loss in the HGOP subjected to longer sonication time. Thus, longer sonication time leads to worse reflection loss of HGOP RASs.

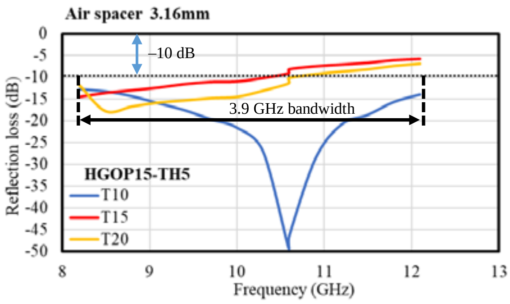

Fig. 6. Effect of sonication time of suspension on reflection loss of HGOP15-TH5-AS3 RASs.

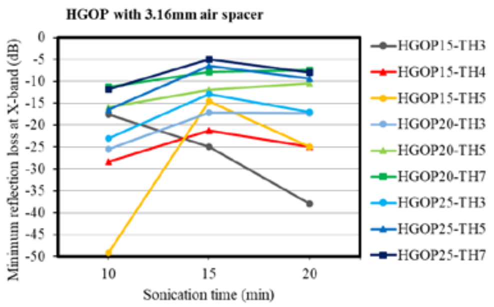

Fig. 7. Effect of sonication time of suspension on reflection loss of 9 kinds of HGOP RASs.

Effect of HGOP Thickness and Loss Mechanisms

Figure 8 shows effect of HGOP thickness on reflection losses of HGOP15–AS3 RAS with two kinds of sonication times. With lowest sonication time 10 min T10 in figure 8(a), reflection loss of HGOP15–T10–AS3 RASs decreases with the increase of HGOP thickness, and best reflection loss peak is – 49.1 dB for HGOP15–T10–TH5–AS3 RAS. In contrast, with highest sonication time 20 min in figure 8(b), reflection loss of HGOP15–T20–AS3 RASs increases with increasing HGOP thickness, and best reflection loss peak is – 38.0 dB for HGOP15–T10–TH3–AS3 RAS. For T10, lower sonication time only breaks GO and RGO nanosheets of HGOP into a few fragments, and proper amount of functional groups of these fragments lead to relaxation of interfacial and dipole polarizations (Peng, 2018). These fragments also increase specific surface area of HGOP. The undulated RGO/void interfaces and RGO/GO interfaces in the HGOP promote interfacial polarization. Relaxation of the polarization results in heat and thus increases dielectric loss. While relaxation of dipole polarization leads to conductive loss, the highly conductive RGOs constitute a network through which micro-current is induced in the alternating electric field. At this moment, the inserted GO with relatively high electrical resistance acts as a resistor, consuming most of the electrical energy. Such processes contribute to the conductive loss. When HGOP thickness increases, both relaxation and conductive loss effects are increased and this lead to better absorbing performance of the RAS.

In contrast, longer sonication time T20 breaks GO and RGO nanosheets into a lot of fragments. Due to many released functional groups of GO, increasing HGOP thickness enhanced its insulation due to very low conductivity of GO. Therefore, microwave tends to penetrate the HGOP instead of inducing dielectric loss, and reduce absorbing performance of the RAS. Figure 9 shows schematic of summarized loss mechanisms of the HGOP RAS for better microwave absorbing performance. HGOP can be recognized as multi-layer and interlocked RGO and GO nanosheets. By optimizing three processing parameters of the HGOP: suspension with lower graphene weight fraction, shorter sonication time, and thicker HGOP, three kinds of loss mechanisms occur including better impedance matching, dielectric loss, and conductive loss. First is caused by lower conductivity of GO in the HGOP that allows microwave to impinge rather than reflect on the HGOP. Second is resulted from better permittivity of the HGOP that transfers the incident microwave into heat. Third, the incident microwave may cause polarization. Defects between RGO and GO nanosheets lead to relaxation of interfacial polarization. Dipole polarization could result in microcurrent in the interlocked RGO/GO, and low conductivity of GO leads to its relaxation. Finally, when the HGOP serves as surface layer of the RAS those loss mechanisms associated with destructive interference by Salisbury screen effect result in efficient energy dissipation of the RAS.

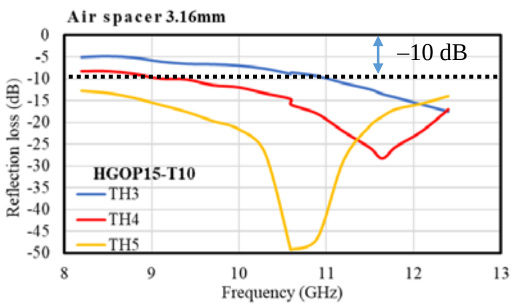

(a)

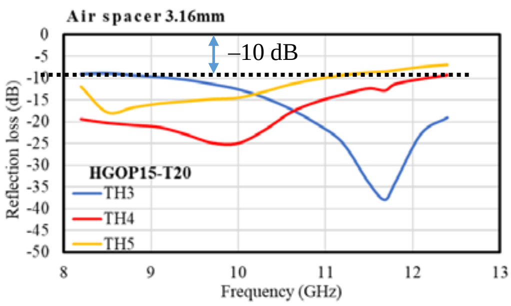

(b)

Fig. 8. Effect of HGOP thickness on reflection loss of (a) HGOP15-T10-AS3 RAS, (b) HGOP15-T20-AS3 RAS.

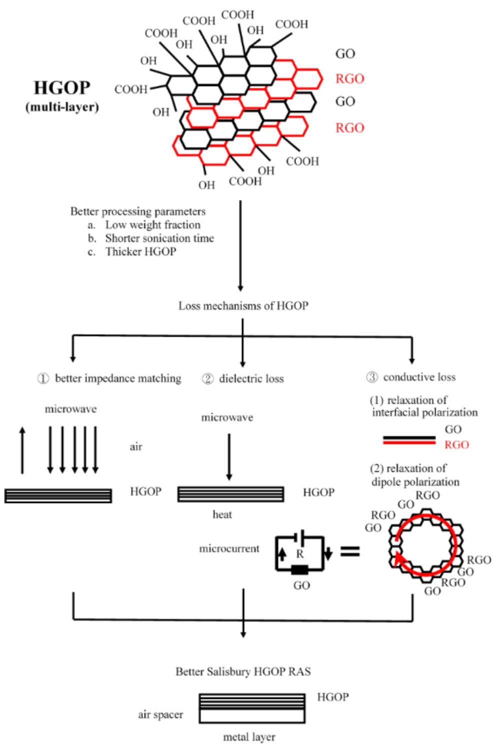

Fig. 9. Schematic of loss mechanisms of the HGOP RAS.

HFSS SIMULATION

In order to conduct Ansys HFSS simulation for reflection loss of the RAS, the electromagnetic (EM) properties (ε', ε'', μ', μ'') of the HGOP absorber are measured by the transmission/reflection loss method. The results of relative complex permittivity ($\varepsilon = \varepsilon' - j\varepsilon''$) and permeability ($\mu = \mu' - j\mu''$) of the representative HGOP15–T10 absorber are shown in figure 10(a) and 10(b), respectively; and the results of HGOP20–T10 absorber are shown in figure 10(c) and 10(d), respectively. For HGOP15–T10 absorber, at a frequency of 8.2 GHz, the real and imaginary parts of complex permittivity are 10.3 and 0.6, respectively, and real part value decreases slightly with increasing frequency. Since this HGOP absorber is a dielectric and dispersive material, its complex permittivity would be frequency-dependent. On the other hand, as shown in figure 10(b) the real and imaginary parts of complex permeability of nonmagnetic HGOP absorber are 1.0 and 0, respectively. With more addition of higher conductive RGOP nanosheets in HGOP20–T10 as shown in figure 10(c), both real and imaginary parts of complex permittivity increase. Adopted proper mathematical equations by the transmission line theory and used the above electromagnetic properties in the HFSS, simulation results of reflection loss of the representative RAS can be achieved and compared with experimental results.

The mathematical equations for the reflection loss of a multiple-layered structure used in HFSS can be derived using transmission line theory. The reflection loss (*RL*) of normal incident EM waves can be expressed as

$$RL = 20\log\left|\frac{Z_2-\eta_0}{Z_2+\eta_0}\right| \tag{1}$$

$$Z_2 = \eta_2\frac{Z_1+\eta_2\tanh(\gamma_2 d_2)}{\eta_2+Z_1\tanh(\gamma_2 d_2)} \tag{2}$$

$$Z_1 = \eta_1\tanh(\gamma_1 d_1) \tag{3}$$

where

$$\eta_i = \eta_0\sqrt{\mu_i/\varepsilon_i} \tag{4}$$

$$\gamma_i = j2\pi f\eta_0\sqrt{\varepsilon_i\mu_i/c}\,,\ i=1,2 \tag{5}$$

In equations (1)-(5), f represents the frequency of incident EM waves, c and η_0 denote the speed and characteristic impedance of free space, respectively. Additionally, d_i, η_i, γ_i, ε_i and μ_i correspond to the thickness, characteristic impedance, propagation constant, complex relative permittivity, and permeability of the *i*th layer of RAS as shown in figure 2.

Figure 11(a) and 11(b) compare the simulation and experimental results of reflection loss of HGOP20–T10–TH4 RASs with glass fiber laminate thickness of 2.85 mm as a spacer, and HGOP15–T10–TH3 RASs with air spacer thickness of 3.16 mm, respectively. In figure 11(a) using glass fiber laminate, the results of simulation and experimental reflection loss peaks are quite consistent. Both have peak value of – 32.9 dB at 9.7 GHz. This indicates that the extracted electromagnetic properties (ε', ε'') of the HGOP20-T10 are consistent with the measured reflection loss of the absorber. While in figure 11(b) using air spacer, simulation reflection loss peak is –42.3 dB at 11.5 GHz, while the experimental reflection loss peak is – 38.0 dB at 11.6 GHz. There is slight inconsistency between simulation and experimental results. Since HGOP is soft and porous, it is not easy to implement in the rectangular waveguide. With this small amount of discrepancy, the trend of simulated results is acceptable. On the other hand, with soft and tailored HGOP, the HGOP RAS is more suitable to fabricate 3D microwave-absorbing structures that can apply to complicated shapes of advanced stealth aircraft or battleships.

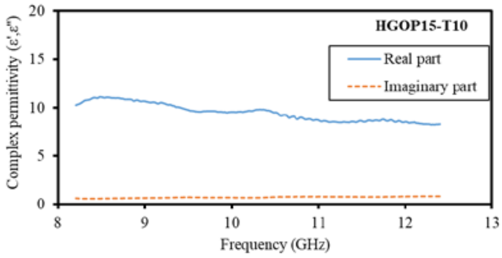

(a)

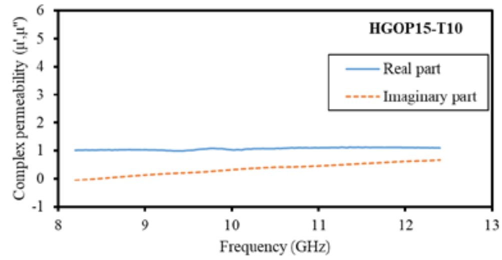

(b)

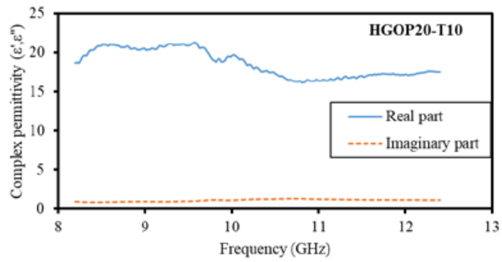

(c)

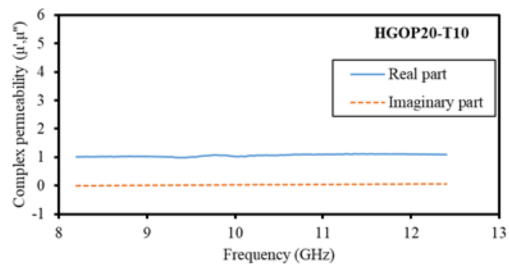

(d)

Fig. 10. (a) Complex permittivity of HGOP15-T10, and (b) complex permeability of HGOP15-T10; (c) complex permittivity of HGOP20-T10, and (d) complex permeability of HGOP20-T10.

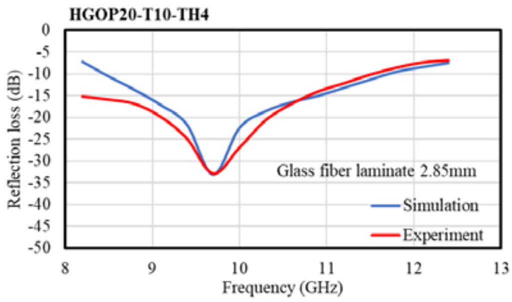

(a)

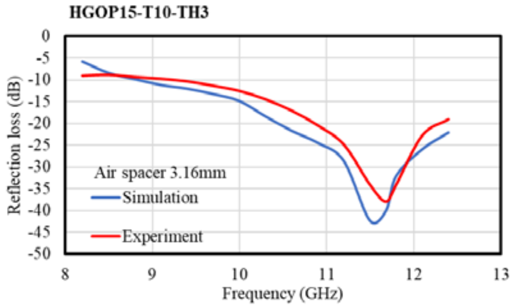

(b)

Fig. 11. Simulation and experimental results of reflection loss of (a) HGOP20-T10-TH4 with glass fiber laminate, and (b) HGOP15-T10-TH3 RASs with air spacer.

CONCLUSIONS

In this work, tailored HGOP radar absorbing structures (RAS) composed of RGO/GO nanosheets are successfully demonstrated. The HGOP RAS not only exhibits excellent and tunable microwave-absorbing (MA) properties, but also could serve as a patch-type radar-absorbing material that is applicable for 3-D curved parts due to the compliant HGOP. The excellent MA properties are caused by adjustable ratio of RGO/GO in suspension. Several interesting findings are summarized. With air spacer thickness of 3.16 mm, the reflection loss of most RASs increases with increasing RGO/GO weight fraction in suspension up to 2.5 wt%. The reflection loss of the RAS increases with increased sonication time for the suspension up to the longest time of 20 min. Longer sonication time may release many oxygen-based functional groups of GO thus makes the HGOP as an insulation that is adverse for dielectric loss. Thickness of HGOP associated with sonication time have a complex effect on reflection loss of the RAS. Higher HGOP thickness and shorter sonication time on suspension lead to better reflection loss due to both relaxations of interfacial and dipole polarizations. Better absorbing performance of the HGOP RAS is synergetically attributed to its dielectric loss, conductive loss, and better impedance matching. Therefore, with RGO/GO of 1.5 wt%, sonication time of 10 min, HGOP thickness around 0.5 mm, and air spacer thickness of 3.16 mm HGOP15–T10–TH5–AS3 RAS has minimum reflection loss of – 49.1 dB at a frequency of 10.6 GHz and good – 10 dB bandwidth of 3.9 GHz. Adopted measured electromagnetic properties of HGOP, simulations of reflection losses of HGOP RASs from Ansys HFSS correlate well with experimental results. Using the glass fiber laminate, both reflection loss peaks from simulation and experimental results are the same as – 32.9 dB at 9.7 GHz. Utilized soft and tailored carbon based HGOP, this innovative HGOP RAS has high potential to be applied to complicated shapes for advanced stealth aircraft or battleships that require high temperature dielectric properties and excellent and adaptable MA performance similar to metamaterials.

ACKNOWLEDGMENTS

Authors are grateful for financial support from National Science and Technology Council (formerly was Ministry of Science and Technology) in Taiwan on this work under contracts NSTC 112-2221-E-035-072 - (Hsien-Kuang Liu) and NSTC 111-2221-E-035-036 (Ruey-Bin Yang).

REFERENCES

Choudhary, H.K., Kumar, R., Pawar, S.P., Bose, S., and Sahoo, B., "Superiority of Graphite Coated Metallic-Nanoparticles over Graphite Coated Insulating-Nanoparticles for Enhancing EMI Shielding,"; *New J. Chem.*, Vol.45, pp. 4592-4600 (2021).

Choudhary, H.K., Kumar, R., Pawar, S.P., Sundararaj, U., and Sahoo, B., "Role of Graphitization-Controlled Conductivity in Enhancing Absorption Dominated EMI Shielding Behavior of Pyrolysis-Derived Fe_3C@C-PVDF Nanocomposites,"; *Mater. Chem. Phys.*, Vol. 263, pp. 124429 (2021).

Choudhary, H.K., Kumar, R., Pawar, S.P., Sundararaj, U., and Sahoo, B., "Enhancing Absorption Dominated Microwave Shielding in Co@C–PVDF Nanocomposites through Improved Magnetization and Graphitization of the Co@C-Nanoparticles,"; *Phys. Chem. Chem. Phys.*, Vol. 21, pp. 15595-15608 (2019).

Chen, C.C., Liang, W.F., Nien, Y.H., Liu, H.K., and Yang, R.B., "Microwave Absorbing Properties of Flake-Shaped Carbonyl Iron/Reduced Graphene Oxide/Epoxy Composites,"; *Mater. Res. Bull.*, Vol. 96, pp. 81-85 (2017).

Dikin, D.A., Stankovich, S., Zimney, E.J., Piner, R.D., Dommett, G.H.B., Evmenenko, G., Nguyen, S.T., and Ruoff, R.S., "Preparation and Characterization of Graphene Oxide Paper,"; *Nature*, Vol. 448, pp. 457-460 (2007).

Houbi, A., Aldashevich, Z.A., Atassi, Y., Telmanovna, Z.B., Saule, M., and Kubanych, K., "Microwave Absorbing Properties of Ferrites and Their Composites: A Review,"; *J. Magn. Magn. Mater.*, Vol. 529, pp. 167839 (2021).

Kumar, R., Choudhary, H.K., Pawar, S.P., Bose, S., and Sahoo, B., "Carbon Encapsulated Nanoscale Iron/Iron-Carbide/Graphite Particles for EMI Shielding and Microwave Absorption,"; *Phys. Chem. Chem. Phys.*, Vol. 19, pp. 23268-23279 (2017).

Li, J., and Zhou, D, "Enhanced Microwave Absorption of Reduced Graphene Oxide/$Ni_{0.4}Zn_{0.4}Co_{0.2}Fe_2O_4$ Composite at Ultrathin Thickness,"; *J. Electron. Mater.*, Vol. 49, pp. 1721-1727 (2020).

Liu, H.K., Yang, R.B., and Yen, K.D., "Radar Absorbing Structures with Reduced Graphene Oxide Papers Fabricated under Various Processing Parameters,"; *J. Electron. Mater.*, Vol. 51, pp. 985-994 (2022).

Liu, H.K., Hwang, S.F., Yang, S.H. and Lei, C.H., "Fatigue Analysis of Graphene Oxide Papers Fabricated under Various Processing Parameters,"; *Fatigue Fract. Eng. Mater. Struct.*, Vol. 43, pp. 2287-2297 (2020).

Liu, H.K., Wang, Y.C., and Huang, T.H., "Moisture Effect on Mechanical Properties of Graphene/Epoxy Nanocomposites,"; *J. Mech.*, Vol. 32, pp. 673-682 (2016).

Meng, F., Wang, H., Huang, F., Guo, Y., Wang, Z., Hui, D., and Zhou, Z., "Graphene-Based Microwave Absorbing Composites: A Review and Prospective,"; *Compos. B: Eng.*, Vol. 137, pp. 260-277 (2018).

Pan, Y.F., Wang, G.S., Liu, L., Guo, L., and Yu, S.H., "Binary Synergistic Enhancement of Dielectric and Microwave Absorption Properties: A Composite of Arm Symmetrical PbS Dendrites and Polyvinylidene Fluoride,"; *Nano Res.*, Vol. 10, pp. 284-294 (2017).

Pang, H., Duan, Y., Huang, L., Song, L., Liu, J., Zhang, T., Yang, X., Liu, J., Ma, X., Di, J., and Liu, X., "Research Advances in Composition, Structure and Mechanisms of Microwave Absorbing Materials,"; *Compos. B. Eng.*, Vol. 224, pp. 109173 (2021).

Park, S., Suk, J.W., An, J., Oh, J., Lee, S., Lee, W., Potts, J.R., Byun, J.H., and Ruoff, R.S., "The Effect of Concentration of Graphene Nanoplatelets on Mechanical and Electrical Properties of Reduced Graphene Oxide Papers,"; *Carbon*, Vol. 50, pp. 4573-4578 (2012).

Peng T., Si Y., Qian J., Zhang Z., Yan X., Zhu C., and Hong X., "Reduced graphene oxide/$MnFe_2O_4$ nanocomposite papers for fast electrical heating and microwave absorption," *Appl. Surf. Sci.*, Vol. 613, pp. 156001 (2023).

Peng, J., Peng, Z., Zhu, Z., Augustine, R., Mahmoud, M.M., Tang, H., Rao, M., Zhang, Y., Li, G., and Jiang, T., "Achieving Ultra-High

Electromagnetic Wave Absorption by Anchoring $Co_{0.33}Ni_{0.33}Mn_{0.33}Fe_2O_4$ Nanoparticles on Graphene Sheets Using Microwave-Assisted Polyol Method,"; *Ceram. Int.*, Vol. 44, pp. 21015-21026 (2018).
Ren, J., Zhang, L., and Fan, X., "Rational Self-Assembly of Fe_3O_4 Nanostructures on Reduced Graphene Oxide for Enhanced Microwave Absorption,"; *J. Electron. Mater.,* Vol. 50, pp. 5057-5071 (2021).
Wang, C., Frogley, M.D., Cinque, G., Liu, L.Q., and Barber, A.H., "Deformation and Failure Mechanisms in Graphene Oxide Paper Using In Situ Nanomechanical Tensile Testing,"; *Carbon,* Vol. 63, pp. 471-477 (2013).
Wen, B., Wang, X.X., Cao, W.Q., Shi, H.L., Lu, M.M., Wang, G., Jin, H.B., Wang, W.Z., Yuan, J., and Cao, M.S., "Reduced Graphene Oxides: the Thinnest and Most Lightweight Materials with Highly Efficient Microwave Attenuation Performances of the Carbon World,"; *Nanoscale*, Vol. 6, pp. 5754-5761 (2014).
Wu, F., Xie, A., Sn, M., Wang, Y., and Wang, M., "Reduced Graphene Oxide (RGO) Modified Spongelke Polypyrrole (PPy) Aerogel for Excellent Electromagnetic Absorption,"; *J. Mater. Chem. A.,* Vol.3, pp. 14358-14369 (2015).
Xu, Y., Luo, J., Yao, W., Xu, J., and Li, T., "Preparation of Reduced Graphene Oxide/Flake Carbonyl Iron Powders/Polyaniline Composites and Their Enhanced Microwave Absorption Properties,"; *J. Alloys Compd.*, Vol. 636, pp. 310-316 (2015).
Yang, R.B., Kuo, W.S., and Lai, H.C., "Effect of Carbon Nanotube Dispersion on the Complex Permittivity and Absorption of Nanocomposites in 2–18 GHz Ranges,"; *J. Appl. Polym. Sci.*, Vol. 131, pp. 40963 (2014).
Zhang, X.J., Wang, G.S., Cao, W.Q., Wei, Y.Z., Liang, J.F., Guo, L., and Cao, M.S., "Enhanced Microwave Absorption Property of Reduced Graphene Oxide (RGO)-$MnFe_2O_4$ Nanocomposites and Polyvinylidene Fluoride,"; *ACS Appl. Mater. Interfaces.*, Vol. 6, pp. 7471-7478 (2014).
Zhang, X.J., Zhu, J.Q., Yin, P.G., Guo, A.P., Huang, A.P., Guo, L., and Wang, G.S., "Tunable High-Performance Microwave Absorption of $Co_{1-x}S$ Hollow Spheres Constructed by Nanosheets within Ultralow Filler Loading,"; *Adv. Funct. Mater.*, Vol. 28, pp. 1800761 (2018).
Zhao, T., Hou, C., Zhang, H., Zhu, R., She, S., Wang, J., Li, T., Liu, Z., and Wei, B., "Electromagnetic Wave Absorbing Properties of Amorphous Carbon Nanotubes,"; *Sci. Rep.*, Vol. 4, pp. 5619 (2014).

混成還原氧化石墨烯紙索爾茲伯里屏吸波器的强化微波吸收研究

劉顯光 吳侑軍
逢甲大學機械與電腦輔助工程學系

楊瑞彬
逢甲大學航太與系統工程學系

摘 要

本論文成功研發一種創新的混成 RGO/GO（還原氧化石墨烯/氧化石墨烯）紙、HGOP，加入索爾茲伯里屏吸波結構中，性能優異。與還原氧化石墨烯紙RGOP相比，HGOP具有可調控的RGO/GO比率，因而具備多個優點，包括：空氣/HGOP間良好的阻抗匹配、具有多重損耗機制。製造HGOP時重要的製程參數包括懸浮液中的RGO/GO重量比率、懸浮液超音波處理時間、和HGOP 的厚度。當RGO/GO 為1.5 wt%、超音波時間為10 分鐘、HGOP 厚度為0.5 mm、空氣層厚度為3.16 mm 時，HGOP15-T10-TH5-AS3 雷達吸波結構（RAS）獲得優異的反射損耗 (RL) 在10.6 GHz 時為 – 49.1 dB，在–10 dB的頻寬為3.9 GHz。為了分析這種新型 RAS所有的損耗機制，我們仔細分析了各種 HGOP 的SEM顯微照片。發現官能基和RGO/GO之交互作用是多重損耗機制的主因。RAS優異的吸波效應，可歸因於HGOP的多種損耗機制、和波的破壞性干涉機制。